Ab Initio Study of Thiolate-Protected Au_{102} Nanocluster

Yi Gao, Nan Shao, and Xiao Cheng Zeng*

Department of Chemistry and Nebraska Center of Materials and Nanoscience, University of Nebraska—Lincoln, Lincoln, Nebraska 68588

ABSTRACT A total structural determination of the $Au_{102}(p\text{-MBA})_{44}$ nanocluster has been recently achieved *via* successful crystallization of the thiolated-protected gold nanocluster (Jadzinsky *et al. Science* 2007, *318*, 430). The embedded Au_{102} cluster may be viewed as a multilayered structure described as Au_{54}(penta-star)@Au_{38}(ten wings)@Au_{10}(two pentagon caps), where the inner Au_{54} "penta-star" consists of five twinned Au_{20} tetrahedral subunits. To gain more insight into high stability of the $Au_{102}(p\text{-MBA})_{44}$ nanocluster, we have performed *ab initio* calculations to study electronic properties of a homologue $Au_{102}(SCH_3)_{44}$ nanocluster, an $Au_{102}(SCH_3)_{42}$ nanocluster (with two SCH_3 groups less), and an "effectively isoelectronic" $Au_{104}(SCH_3)_{46}$ nanocluster with a more symmetric embedded Au_{104} structure. Electronic structure calculations suggest that the $Au_{102}(SCH_3)_{44}$ nanocluster possesses a reasonably large gap (~0.54 eV) between the highest occupied molecular orbital and the lowest unoccupied molecular orbital (HOMO—LUMO gap), which is comparable to the measured HOMO—LUMO gap (~0.65 eV) of the bare Au_{58} cluster. Likewise, the $Au_{104}(SCH_3)_{46}$ nanocluster has a HOMO—LUMO gap of ~0.51 eV, comparable to that of $Au_{102}(SCH_3)_{44}$ nanocluster. In contrast, the $Au_{102}(SCH_3)_{42}$ nanocluster has a zero HOMO—LUMO gap. These results confirm that high stability of the $Au_{102}(p\text{-MBA})_{44}$ nanocluster may be attributed in part to the electronic shell closing of effective 58 (= 102 − 44) valence electrons, as in the case of $Au_{25}(SCH_2CH_2Ph)_{18}^-$ cluster whose high stability may be attributed to the electronic shell closing of effective 8 (= 26 −18) valence electrons.

KEYWORDS: gold nanoclusters · thiolate protection · Jellium model · HOMO—LUMO gap · shell closing

Gold nanoclusters have attracted considerable attention owing to their unique catalytic and electronic properties, as well as their great potential for industrial applications.[1–5] Advances have been made over the past few years in resolving structures of small-to-medium sized gold clusters.[6–18] For example, it has been established from joint experimental—theoretical studies that anion gold clusters Au_4^-—Au_{12}^- exhibit two-dimensional (2D) planar structures,[7–9] Au_{16}^-—Au_{18}^- possess hollow cage structures,[10,11] Au_{20}^- has a distinct tetrahedral structure (the smallest gold pyramid),[12] Au_{24}^- exhibits a tube-like structure,[11,13] and Au_{25}^-,[14] Au_{32}^-,[15] and Au_{34}^-[16,17] exhibit core—shell structures. Beyond the size of Au_{34}, however, atomic structures of gold nanoclusters are largely unknown, except Au_{55}^-—Au_{64}^-.[18–20] Indeed, it is still a challenging task to determine total structures of bare gold clusters solely from experiment, particularly for clusters in the size range of 1—3 nm. For larger-sized gold nanoparticles (*e.g.*, > 3 nm), their structures can be directly inferred from common structural characterization techniques such as high-resolution transmission electron microscopy, scanning tunneling microscopy, atomic force microscopy, and small-angle X-ray scattering.

Ligand-protected gold nanoclusters[21–25] provide alternative building blocks to fabricate new forms of matter such as cluster-assembled arrays.[26] Previous *ab initio* theoretical studies have provided molecular insight into thiolate—gold interaction.[27–36] Recently, a major breakthrough in total structure determination of a thiolate-protected gold nanocluster has been achieved by Jadzinsky *et al.*[37] These researchers have successfully produced a single crystal of the gold—thiolate nanocluster, each being composed of exactly 102 Au atoms and 44 *p*-mercaptobenzoic acid (*p*-MBA) groups (Figure 1). The 44 thiolate groups form the so-called "staple" motifs on the surface. The embedded Au_{102} structure may be viewed as a 49 atom Marks decahedral core covered by two 20 atom caps on opposite poles (with C_5 symmetry), plus 13 equatorial Au atoms.[37] Another structural description, given by Whetten and Price,[38] is that the embedded Au_{102} structure is composed of a grand core of 79 Au atoms plus 23 exterior Au atoms. The grand core consists of a 49 atom Marks decahedral cluster and two groups of 15 Au atoms located on opposite poles. Thus, the 49 atom Marks decahedral cluster can be viewed as a

*Address correspondence to xczeng@phase2.unl.edu.

Received for review May 5, 2008 and accepted June 18, 2008.

Published online June 27, 2008.
10.1021/nn800268w CCC: $40.75

© 2008 American Chemical Society

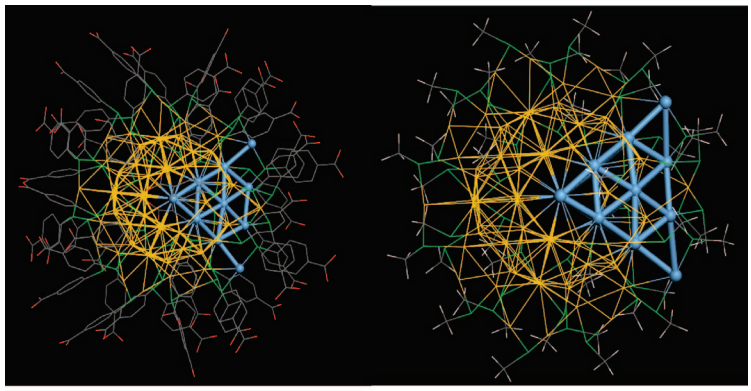

(a) (b)

Figure 1. (a) Atomic structure of synthesized Au_{102}(*p*-MBA)$_{44}$ nanocluster (in crystalline form; ref 37). (b) Optimized structure of a $Au_{102}(SCH_3)_{44}$ nanocluster. Yellow (blue): Au; green: S; gray: C; red: O; and white: H. Blue highlights one of five twinned Au_{20} tetrahedral subunits.

structural motif for the thiolate-protected nanocluster. The 23 exterior Au atoms serve only to connect the thiolate groups with the 79 Au atom grand core.

It has been known that truncated decahedral motifs with 5-fold symmetry are prevalent structural motifs for passivated gold nanoclusters in the 1−2 nm size range.[39] Still it is interesting to study the reason why this thiolate-protected gold nanocluster contains 102 gold atoms. One important factor pointed out by Jadzinsky *et al.* is that high stability of the thiolate-protected Au_{102} nanocluster is due in part to the closure of the electronic shell. Each of the 102 Au atoms donates one valence electron, while each of the 44 thiolates accepts one electron (or each thiolate has a formal charge of −1). Effectively, the number of nonlocalized valence electrons is 102 − 44 = 58. According to the spherical Jellium model,[40−43] bare alkaline or noble metal clusters with 2, 8, 20, 34, 58, 92, *etc.* valence electrons should be highly stable because of closure of the electronic shell.[44,45] Indeed, the spherical Jellium model has been very successful in explaining high stability of several "magic number" gold clusters such as Au_8, Au_{20}, Au_{34}, and Au_{58}.[12,16,17,19,20] In general, noble metal clusters with a closed electronic shell possess a relatively large energy gap between the highest occupied molecular orbital and the lowest unoccupied molecular orbital (HOMO−LUMO gap). For example, the tetrahedral cluster T_d−Au_{20}, core/shell cluster Au_{34}, as well as core/shell cluster Au_{58} exhibit a measured HOMO−LUMO gap of 1.77,[12] 0.94,[16,17] and 0.65 eV,[19,20] respectively. Very recently, three groups[44−46] have shown that a thiolate-protected anion gold cluster $Au_{25}(SCH_2CH_2Ph)_{18}^-$ (with an icosahedral Au_{13} core) has a large HOMO−LUMO gap of ~1.2 eV. The $Au_{25}(SCH_2CH_2Ph)_{18}^-$ cluster may be viewed as having effective eight nonlocalized valence electrons, which is a magic number according to the spherical Jellium model. On the other hand, the $Au_{38}(SR)_{24}$ cluster has a smaller HOMO−LUMO gap (0.9 eV) than that of $Au_{25}(SCH_2CH_2Ph)_{18}^-$.[47−54] This behavior might be explained with a nonspherical shell model.[53]

Despite numerous theoretical studies on small and medium-sized thiolate-protected gold clusters, few *ab initio* studies have been found in the literature on large-size thiolate-protected gold clusters. In this article, we present a comprehensive *ab initio* study and structural analysis of a homologue $Au_{102}(SCH_3)_{44}$ nanocluster, an $Au_{102}(SCH_3)_{42}$ nanocluster with the same number of Au atoms but two thiolate groups less, as well as an "effectively isoelectronic" $Au_{104}(SCH_3)_{46}$ nanocluster with a more symmetric embedded Au_{104} structure. Electronic structure calculations show that the $Au_{102}(SCH_3)_{44}$ nanocluster has a HOMO−LUMO gap of 0.56 eV, comparable to that of bare Au_{58} cluster, while the $Au_{104}(SCH_3)_{46}$ nanocluster has a HOMO−LUMO gap of 0.51 eV. However, the $Au_{102}(SCH_3)_{42}$ nanocluster has a zero HOMO−LUMO gap. Hence, our *ab initio* calculations confirm that the spherical Jellium model is likely applicable to thiolate-protected noble metal clusters and that high stability of thiolate-protected Au_{102} nanoclusters is most likely due to closure of the electronic shell.

RESULTS AND DISCUSSION

Structural Anatomy. First, we present a structure analysis of the embedded Au_{102} structure in the same fashion as Mednikov *et al.*'s analysis for a ligated 165 atom multishell Pd−Pt nanocluster.[55] In Figure 1a,b, we display atomic structure of the experimental Au_{102}(*p*-MBA)$_{44}$ nanocluster and optimized structure of the $Au_{102}(SCH_3)_{44}$ nanocluster, respectively. Despite differences in their ligands, the embedded Au_{102} structures in both thiolate-protected nanoclusters are very similar. The similarity can be more clearly seen from **2a** and **2b** in Figure 2a, where exterior ligands are removed for ease of view. The structural similarity in embedded Au_{102} structures suggests that the ligand−gold interaction in the Au_{102}(*p*-MBA)$_{44}$ and its homologue $Au_{102}(SCH_3)_{44}$ nanocluster is more or less the same. Hence we expect that electronic properties of the $Au_{102}(SCH_3)_{44}$ nanocluster can be useful to assess electronic properties of the larger Au_{102}(*p*-MBA)$_{44}$ nanocluster. We have also performed structural optimization for a bare Au_{102} cluster carved out from the experimental Au_{102}(*p*-MBA)$_{44}$ nanocluster (**2c** in Figure 2a). After structural optimization, the bare Au_{102} cluster becomes slightly more ordered with quasi-5-fold symmetry, although it does not have exact C_5 symmetry due to the existence of two triangle wings (see below). Jadzinsky *et al.* have pointed out that the 49 atom Marks decahedral Au cluster may be viewed as five twinned crystals.[37] As shown in Figure 3, if additional five vertexes Au atoms are included together with the 49 atom truncated decahedron, a 54 atom "perfect" decahedral structure is seen, which can be also viewed as five twinned Au_{20}

tetrahedral subunits (Figure 3b). Hereafter, the decahedral Au_{54} structure is named as a *penta-star*. In Figure 2b, rotational angle distribution in the region S1−S5 of **2a**−**2c** is compared with that of a perfect D_{5h} structure. It is clear that **2c** gives the best match with perfect D_{5h} structure, while **2a** and **2b** are not deviated too much from the perfect D_{5h} structure. In principle, one could also study shear-strain distribution within the S1−S5 region, as shown in a recent study for much larger decahedral Au nanoparticles.[56] Previous studies have shown that bare decahedral Au nanoparticles with a size <10 nm are unstable because the twinned decahedral Au nanoparticles are intrinsically strained.[57,58] Here, the five tetrahedral subunits within a Au_{54} penta-star share a single edge coinciding with the 5-fold axis. Although a perfect T_d−Au_{20} tetrahedral cluster is highly stable due to closure of the electronic shell,[12] five perfect T_d−Au_{20} clusters cannot completely form a perfect penta-star. As illustrated in Figure 3a, if two vertexes (*e.g.*, a and c) of a T_d−Au_{20} cluster are connected through the midpoint of opposing edge (point b), the angle ∠abc is 70.53°. When five T_d−Au_{20} subunits are joined together, there is 7.35° (= 360 − 5 × 70.53) solid-angle deficiency. Hence, a stand-alone Au_{54} penta-star is energetically unfavorable due to large strain. On the other hand, the presence of a Au_{54} penta-star within the Au_{102}(*p*-MBA)$_{44}$ nanocluster indicates that decahedral structure can be energetically favorable in thiolate-protected gold nanoclusters with size as small as 2 nm.

With the Au_{49} Marks decahedron as the core, growth of thiolate-protected Au nanocluster is expected to be strongly affected by local thiolate−gold interaction. Jadzinsky *et al.*[37] have demonstrated that all thiolate groups bound to the gold cluster are in the form of either *RS-Au-SR* simple "staple" motif (totally 19) or *RS-Au-SR-Au-SR* extended "staple" motif (totally 2). Indeed, each of the five vertexes of the Au_{54} penta-star is part of the *RS-Au-SR* staple motif, growing based on the Marks decahedral Au_{49} core. Ultimately, formation of a highly stable Au_{102}(*p*-MBA)$_{44}$ nanocluster manifests a delicate balance between local thiolate−gold interaction (in the form of staple motifs), with the growth mode compatible with underlying Marks decahedral Au_{49} core, and an overall tendency to close the electronic shell. Our structural analysis indicates that the requirement of forming 46 *RS*-Au bonds (out of total 88 *RS*-Au bonds) leads to five wings on each side of the Au_{54} penta-star (Figure 3b). The 10 wings include eight rhombuses and two triangles (blue), taking 38 Au atoms. The formation of two triangle wings breaks 5-fold symmetry associated with the Au_{54} penta-star. The 13 equatorial Au atoms can be divided into two groups: 5 as the corner of the Au_{54} penta-star, and 8 as the corner of the wings.

On top of the 10 wings, the requirement of forming 10 additional staple motifs (including 20 *RS*-Au bonds) results in an additional five-atom pentagonal cap on each side of the Au_{54} penta-star. Hence the embedded Au_{102} structure may be also viewed as a multilayer

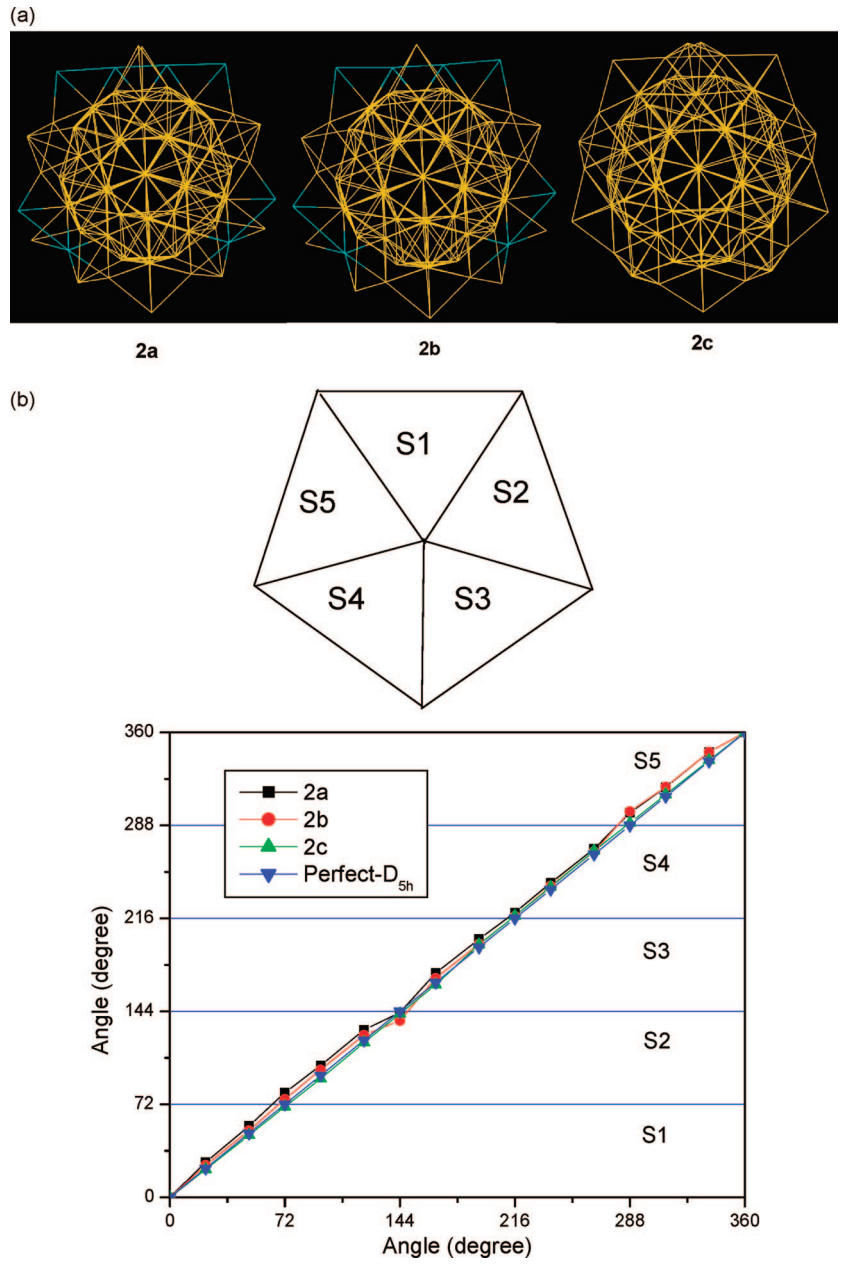

Figure 2. Embedded Au_{102} structures. (a) 2a: Original structure derived from the synthesized Au_{102}(*p*-MBA)$_{44}$ (ref 37); 2b: carved out from optimized $Au_{102}(SCH_3)_{44}$ nanocluster; 2c: optimized bare Au_{102} cluster whose initial configuration is the same as 2a. Blue "bonds" are merely a guide to the eye as these bonds are longer than typical Au−Au bond length. (b) Rotational angle distribution of 2a, 2b, and 2c *versus* that of perfect D_{5h} structure.

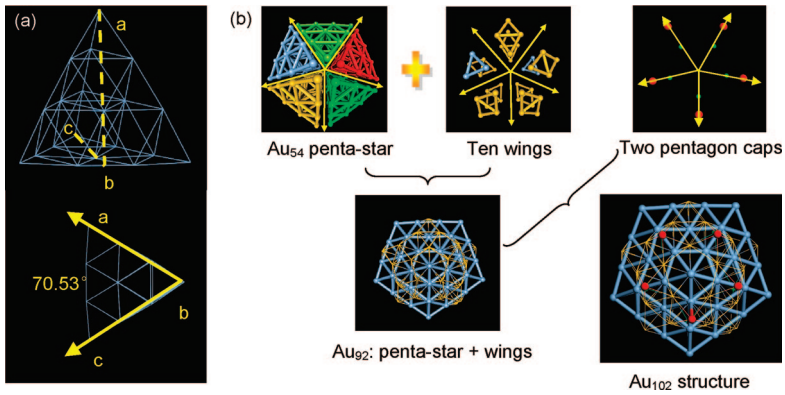

Figure 3. (a) Perfect tetrahedral T_d−Au_{20}; ∠abc = 70.53°. (b) Graphitic *anatomy* of embedded Au_{102} structure. A Au_{54} *penta-star* consists of five twinned Au_{20} tetrahedral subunits (in five colors). Ten wings (taking 38 Au atoms) include 8 rhombuses and 2 triangles (in blue), 5 on each side of the penta-star. The Au_{54} *penta-star* (in blue) plus the wings (in yellow) form a Au_{92} structure. Adding a five-atom pentagonal cap (in red and green) on each side of the Au_{92} gives rise to the Au_{102} structure.

structure described by Au_{54}(penta-star)@Au_{38}(ten wings)@Au_{10}(two caps) (Figure 3b). Lastly, the remaining required 22 *RS*-Au bonds (= 88 − 46 − 20) stem from 15 perimeter Au atoms of the Au_{54} penta-star. Among these 15 Au atoms, the five vertex Au atoms and two Au atoms on edges are all connected with two *RS* groups.

Electronic Properties. The DFT method is used to compute electronic structures of bare Au_{102} cluster (**2c** in Figure 2a) as well as thiolate-protected nanoclusters. It is found that bare Au_{102} clusters possess a relatively small HOMO−LUMO gap (~0.16 eV), whereas the $Au_{102}(SCH_3)_{44}$ nanocluster has notably a larger HOMO−LUMO gap (0.54 eV), indicating that the thiolate-protected Au_{102} nanocluster is more chemically stable than bare Au_{102} clusters. Moreover, a HOMO−LUMO gap of 0.54 eV is comparable to that (~0.65 eV) of bare Au_{58} clusters (measured from anion photoelectron spectroscopy experiment[19,20]). The appreciable HOMO−LUMO gap of bare Au_{58} clusters can be understood based on the spherical Jellium model in that 58 valence electrons of a Au_{58} cluster close the electronic shell. Likewise, the fact that the $Au_{102}(SCH_3)_{44}$ nanocluster also exhibits a reasonably large HOMO−LUMO gap supports an assumption that the Jellium model may be also applicable to the thiolate-protected noble metal clusters.

To provide another evidence for applicability of the Jellium model to thiolate-protected noble metal clusters, we constructed a $Au_{104}(SCH_3)_{46}$ nanocluster (based on the $Au_{102}(SCH_3)_{44}$ nanocluster) which contains an embedded Au_{104} structure with 5-fold symmetry. As mentioned above, the Au_{102} structure contains two triangle wings so that it no longer has 5-fold symmetry. By replacing the two triangle wings with two rhombus wings, 5-fold symmetry can be restored. The newly constructed Au_{104} structure can be described as Au_{54}(penta-star)@Au_{40}(ten rhombus wings)@Au_{10}(two pentagon caps). Moreover, by connecting two new SCH_3 ligands with added gold atoms to form two simple "staple" motifs, we obtain a new $Au_{104}(SCH_3)_{46}$ nanocluster (Figure 4). Electronic structure calculations show that optimized $Au_{104}(SCH_3)_{46}$ nanocluster exhibits a HOMO−LUMO

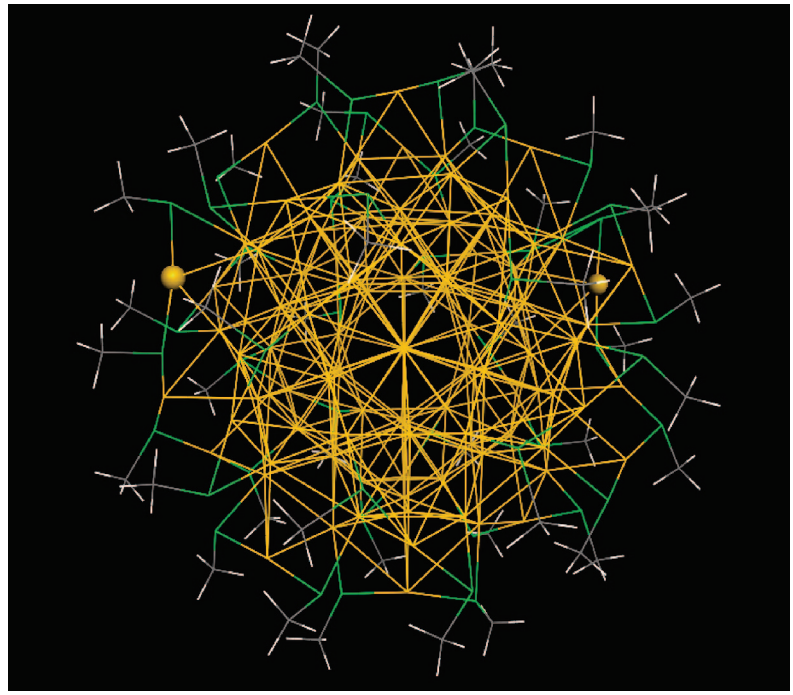

Figure 4. Optimized atomic structure of a $Au_{104}(SCH_3)_{46}$ nanocluster. Yellow: Au; green: S; gray: C; and white: H. Two spheres represent the two newly added Au atoms based on the $Au_{102}(SCH_3)_{44}$ nanocluster.

gap of ~0.51 eV, comparable to that (0.54 eV) of the $Au_{102}(SCH_3)_{44}$ nanocluster. Again, this 0.54 eV HOMO−LUMO gap with the $Au_{104}(SCH_3)_{46}$ nanocluster is likely due to electronic shell closing of effective 58 (= 104 − 46) valence electrons. As an independent test, we removed two SCH_3 ligands from the original $Au_{102}(SCH_3)_{44}$ nanocluster and obtained a $Au_{102}(SCH_3)_{42}$ nanocluster. DFT calculations show that this $Au_{102}(SCH_3)_{42}$ nanocluster has a zero HOMO−LUMO gap. The latter may be explained by the fact that the cluster has effective 60 (= 102 − 42) valence electrons (open shell).

Additionally, we performed electronic structure calculations for the $Au_{25}(SCH_3)_{18}^-$ "magic number" cluster.[44–46] This anion may be viewed to have effective 8 nonlocalized valence electrons (25 − 18 + 1 = 8), whereas the cation counterpart $Au_{25}(SCH_3)_{18}^+$ has effective 6 nonlocalized valence electrons (25 − 18 − 1 = 6). Interestingly, the calculated HOMO−LUMO gap of the $Au_{25}(SCH_3)_{18}^-$ cluster is 1.2 eV, much larger that that (0.6 eV) of the $Au_{25}(SCH_3)_{18}^+$ cluster. In summary, the spherical Jellium model which has been so successful in explaining magic number clusters of bare alkaline and noble metal clusters is possibly applicable to thiolate-protected gold clusters.

Hirshfield charge analysis suggests that a small charge transfer occurs from Au atoms to S atoms. On the surface of the embedded Au_{102} cluster, Au atoms can be categorized into three groups: group 1 has no coordination with any S atoms; group 2 has coordination with a single S atom; and group 3 has coordination with two S atoms. For group 1, each Au atom undertakes a little negative charge (~ −0.0025e). For group 2, every Au atom donates 0.024−0.031e to the S atom. For group 3, every Au atom donates 0.058−0.081e to the S atoms, consistent with previous theoretical results.[28–31] Meanwhile, every S atom takes −0.035 to −0.045e, and the C atom of the methyl group takes −0.117 to −0.123e. In Figure 5a, a plot of the molecular electrostatic potential (MEP) offers a global view of electric charge distribution over surface of the $Au_{102}(SCH_3)_{44}$ nanocluster. It can be seen that methyl groups, group 2, and group 3 Au atoms exhibit highly positive MEP (blue), whereas sulfur atoms and group 1 Au atoms exhibit negative MEP, consistent with the Hirshfield charge analysis. Molecular orbital hybridization is another common characteristic of ligand-protected metal nanoclusters. As an independent test, we performed an Hirshfield charge analysis for the $Au_{25}(SCH_3)_{18}^-$ cluster and obtained qualitatively similar results of charge transfer as those for the $Au_{102}(SCH_3)_{44}$ nanocluster. Total charge transfer from Au to S is 0.62e for the $Au_{25}(SCH_3)_{18}^-$ cluster compared to 2.87e for the $Au_{102}(SCH_3)_{44}$ nanocluster. Both calculations suggest that charge transfer may not play a key role in reducing the effective number of valence electrons neither in the $Au_{102}(SCH_3)_{44}$ nanocluster nor in the $Au_{25}(SCH_3)_{18}^-$ cluster. Rather, it seems that those Au atoms involved in the staple motifs no longer contribute to effective number of nonlocalized valence electrons in the sense of the spherical Jellium model. As such, for a $Au_m(SCH_3)_n$ cluster, its effective number of valence electrons may be given by $m - n$. Figure 5b displays calculated HOMO and LUMO of the $Au_{102}(SCH_3)_{44}$ nanocluster. It can be seen that both HOMO and LUMO are largely contributed by the 3p orbital of S atoms as well as the 6s and 5p orbitals of the Au atoms in the staple motifs, supporting localization of certain Au s-valence electrons due to formation of the staple motifs.

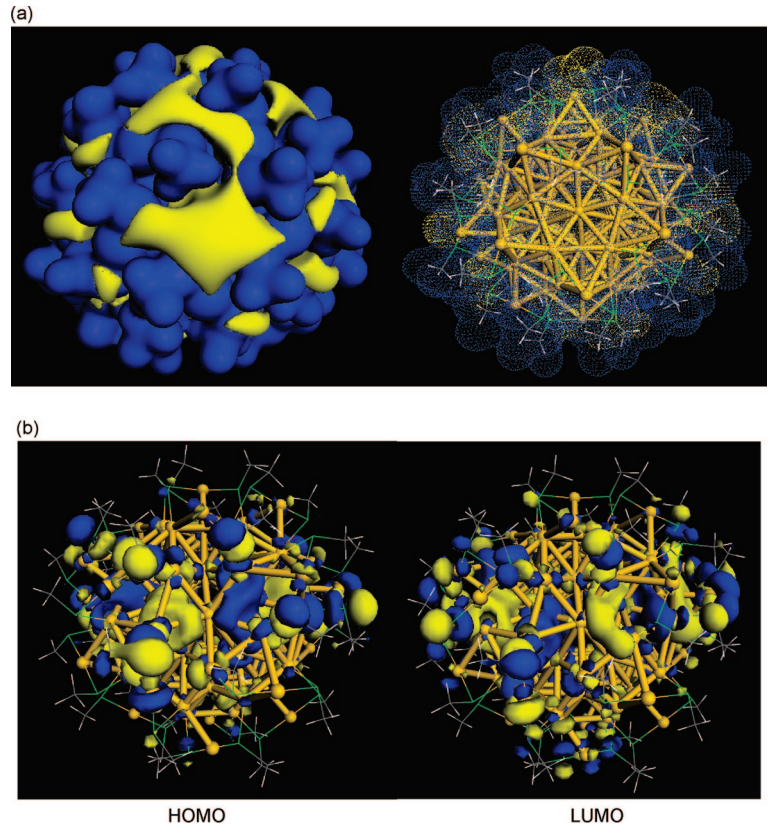

Figure 5. (a) Plot of an isosurface of eletrostatic potential for the $Au_{102}(SCH_3)_{44}$ nanocluster (left: solid model; right: dot model; yellow: negative; blue: positive). (b) Isosurface (the isovalue is 0.01 au) of the HOMO (left) and LUMO (right) of the $Au_{102}(SCH_3)_{44}$ nanocluster. Blue and yellow denote positive and negative sign of wave functions, respectively.

CONCLUSION

We have performed an *ab initio* study of a $Au_{102}(SCH_3)_{44}$ nanocluster which is a homologue to the recently synthesized $Au_{102}(p\text{-MBA})_{44}$ nanocluster and an "effective isoelectronic" $Au_{104}(SCH_3)_{46}$ with a more symmetric embedded Au_{104} structure, as well as a $Au_{102}(SCH_3)_{42}$ nanocluster with two less thiolate groups than $Au_{102}(SCH_3)_{44}$. Electronic structure

calculations show that the $Au_{102}(SCH_3)_{44}$ nanocluster exhibits a modest HOMO−LUMO gap (~0.54 eV), comparable to that (~0.65 eV) of the bare Au_{58} cluster, while the $Au_{104}(SCH_3)_{46}$ nanocluster has a HOMO−LUMO gap of ~0.51 eV, comparable to that of $Au_{102}(SCH_3)_{44}$. In contrast, the $Au_{102}(SCH_3)_{42}$ nanocluster exhibits a zero HOMO−LUMO gap. These results support an explanation that high stability of the synthesized $Au_{102}(p\text{-MBA})_{44}$ nanocluster is likely due to electronic shell closing of effective 58 valence electrons. Charge analysis shows that little charge transfer occurs between embedded Au_{102} structure and thiolate groups. Thus, the effective number of valence electrons (58 = 102 − 44) may be attributed to localization of Au s-valance electrons (44) due to formation of 19 simple and 2 extended "staple" motifs. Likewise, high stability of the $Au_{25}(SCH_2CH_2Ph)_{18}^-$ cluster may be attributed to electronic shell closing of effective 8 valence electrons. In general, for a $Au_m(SCH_3)_n$ cluster, its effective number of valence electrons may be given by $m - n$. In particular, high stability of thiolate-protected gold nanoclusters such as $Au_{102}(p\text{-MBA})_{44}$ and $Au_{25}(SCH_2CH_2Ph)_{18}^-$ is a manifestation of a delicate interplay between local thiolate−gold interaction (in the form of staple motifs), a growth process compatible with underlying Au core symmetry (Marks decahedral Au_{49} core for $Au_{102}(p\text{-MBA})_{44}$, and icosahedral Au_{13} core for $Au_{25}(SCH_2CH_2Ph)_{18}^-$), as well as a global tendency of closing the electronic shell.

METHODS

Atomic coordination of the $Au_{102}(p\text{-MBA})_{44}$ nanocluster was obtained from the authors of ref 37. For computational feasibility, we studied a smaller homologue gold nanocluster, $Au_{102}(SCH_3)_{44}$. We used a density functional theory (DFT) method to perform full geometric optimization of bare Au_{102} structures and thiolate-protected nanoclusters. Similar DFT methods have been used by others in their studies of smaller-sized thiolate-protected gold nanoclusters such as $Au_{25}(SCH_3)_{18}^-$ and $Au_{38}(SCH_3)_{24}$.[28–31,44–46] The generalized gradient approximation in the form of the Perdew−Wang 91 functional,[59] a relativistic effective core potential (ECP), and the double-numerical polarized basis set (DNP) implemented in the DMol3 software package[60,61] were employed in the DFT calculation. To validate the computation method, we optimized the tetrahedral T_d−Au_{20} cluster and obtained a computed HOMO−LUMO gap of 1.80 eV, which is in good agreement with measured HOMO−LUMO gap of 1.77 eV.[12]

Acknowledgment. We thank Yong Pei for valuable discussion. This work was supported by grants from NSF (CHE and CMMI), DOE (DE-FG02-04ER46164), and the Nebraska Research Initiative, and by the Research Computing Facility at University of Nebraska—Lincoln and the Holland Computing Center at University of Nebraska—Omaha.

REFERENCES AND NOTES

1. Haruta, M. Size- and Support-Dependency in the Catalysis of Gold. *Catal. Today* **1997**, *36*, 153–166.
2. Bond, G. C.; Louis, C.; Thompson, D. T. *Catalysis by Gold*; Imperial College Press: London, 2006.
3. Schwarz, H. Relativistic Effects in Gas-Phase Ion Chemistry: An Experimentalist's View. *Angew. Chem., Int. Ed.* **2003**, *42*, 4442–4454.
4. Daniel, M. C.; Astruc, D. Gold Nanoparticles: Assembly, Supramolecular Chemistry, Quantum-Size-Related Properties, and Applications toward Biology, Catalysis, and Nanotechnology. *Chem. Rev.* **2004**, *104*, 293–346.
5. Schmid, G.; Bäumle, M.; Geerkens, M.; Heim, I.; Osemann, C.; Sawitowski, T. Current and Future Applications of Nanoclusters. *Chem. Soc. Rev.* **1999**, *28*, 179–185.
6. Pyykkö, P. Theoretical Chemistry of Gold. *Angew. Chem., Int. Ed.* **2004**, *43*, 4412–4456.
7. Häkkinen, H.; Landman, U. Gold Clusters (Au_N, $2 \leq N \leq 10$) and Their Anions. *Phys. Rev. B* **2000**, *62*, R2287–2290.
8. Furche, F.; Ahlrichs, R.; Weis, P.; Jacob, C.; Glib, S.; Bierweiler, T.; Kappes, M. M. The Structures of Small Gold Cluster Anions as Determined by a Combination of Ion Mobility Measurements and Density Functional Calculations. *J. Chem. Phys.* **2002**, *117*, 6982–6990.
9. Häkkinen, H.; Yoon, B.; Landman, U.; Li, X.; Zhai, H. J.; Wang, L.-S. On the Electronic and Atomic Structures of Small Au_N^- ($N = 4-14$) Clusters: A Photoelectron Spectroscopy and Density-Functional Study. *J. Phys. Chem. A* **2003**, *107*, 6168–6175.
10. Bulusu, S.; Li, X.; Wang, L.-S.; Zeng, X.-C. Evidence of Hollow Golden Cages. *Proc. Natl. Acad. Sci. U.S.A.* **2006**, *103*, 8326–8330.
11. Xing, X.; Yoon, B.; Landman, U.; Parks, J. H. Structural Evolution of Au Nanoclusters: From Planar to Cage to Tubular Motifs. *Phys. Rev. B* **2006**, *74*, 165423.
12. Li, J.; Li, X.; Zhai, H.-J.; Wang, L.-S. Au_{20}: A Tetrahedral Cluster. *Science* **2003**, *299*, 864–867.
13. Yoon, B.; Koskinen, P.; Huber, B.; Kostko, B.; v. Issendorff, B.; Häkkinen, H.; Moseler, M.; Landman, U. Size-Dependent Structural Evolution and Chemical Reactivity of Gold Clusters. *ChemPhysChem* **2007**, *8*, 157–161.
14. Bulusu, S.; Li, X.; Wang, L.-S.; Zeng, X.-C. Structural Transitions from Pyramidal to Fused Planar to Tubular to Core/Shell Compact in Gold Clusters: Au_n^- ($n = 21-25$). *J. Phys. Chem. C* **2007**, *111*, 4190–4198.
15. Ji, M.; Gu, X.; Li, X.; Gong, X.; Li, J.; Wang, L.-S. Experimental and Theoretical Investigation of the Electronic and Geometrical Structures of the Au_{32} Cluster. *Angew. Chem., Int. Ed.* **2005**, *44*, 7119–7123.
16. Lechtken, A.; Schooss, D.; Stairs, J. R.; Blom, M. N.; Furche, F.; Morgner, N.; Kostko, O.; von Issendorff, B.; Kappes, M. M. Au_{34}: A Chiral Gold Cluster. *Angew. Chem., Int. Ed.* **2007**, *46*, 2944–2948.
17. Gu, X.; Bulusu, S.; Li, X.; Zeng, X.-C.; Li, J.; Gong, X.-G.; Wang, L.-S. Au_{34}: A Fluxional Core−Shell Cluster. *J. Phys. Chem. C* **2007**, *111*, 8228–8232.
18. Garzon, I. L.; Michaelian, K.; Beltran, M. R.; Posada-Amarillas, A.; Ordejon, P.; Artacho, E.; Sanchez-Portal, D.; Soler, J. M. Lowest Energy Structures of Gold Nanoclusters. *Phys. Rev. Lett.* **1998**, *81*, 1600–1604.
19. Häkkinen, H.; Moseler, M.; Kostko, O.; Morgner, N.; Hoffmann, M. A.; von Issendorff, B. Symmetry and Electronic Structure of Noble-Metal Nanoparticles and the Role of Relativity. *Phys. Rev. Lett.* **2004**, *93*, 093401.
20. Huang, W.; Ji, M.; Dong, C.-D.; Gu, X.; Wang, L.-M.; Gong, X. G.; Wang, L.-S. Relativistic Effects and the Unique Low-Symmetry Structures of Gold Nanoclusters. *ACS Nano* **2008**, *2*, 897–904.
21. Brust, M.; Walker, M.; Bethell, D.; Schiffrin, D. J.; Whyman, R. J. Synthesis of Thiol-Derivatized Gold Nanoparticles in a 2-Phase Liquid−Liquid System. *J. Chem. Soc., Chem. Commun.* **1994**, *7*, 801–802.
22. Brust, M.; Fink, J.; Bethell, D.; Schiffrin, D. J.; Kiely, C. J. Synthesis and Reactions of Functionalized Gold Nanoparticles. *J. Chem. Soc., Chem. Commun.* **1995**, *16*, 1655–1656.

23. Leff, D. V.; Ohara, P. C.; Heath, J. R.; Gelbart, W. M. Thermodynamic Control of Gold Nanocrystal Size—Experiments and Theory. *J. Phys. Chem.* **1995**, *99*, 7036–7041.
24. Templeton, A. C.; Wuelfing, W. P.; Murray, R. W. Monolayer-Protected Cluster Molecules. *Acc. Chem. Res.* **2002**, *33*, 27–36.
25. Schmid, G.; Corain, B. Nanoparticulated Gold: Syntheses, Structures, Electronics, and Reactivities. *Eur. J. Inorg. Chem.* **2003**, *17*, 3081–3098.
26. Whetten, R. L.; Shafigullin, M. N.; Khoury, J. T.; Schaaff, T. G.; Vezmar, I.; Alvarez, M. M.; Wilkinson, A. Crystal Structures of Molecular Gold Nanocrystal Arrays. *Acc. Chem. Res.* **1999**, *32*, 397–406.
27. Maksymovych, P.; Sorescu, D. C., Jr. Gold-Adatom-Mediated Bonding in Self-Assembled Short-Chain Alkanethiolate Species on the Au(111) Surface. *Phys. Rev. Lett.* **2006**, *97*, 146103.
28. Grönbeck, H.; Häkkinen, H. Polymerization at the Alkylthiolate−Au(111) Interface. *J. Phys. Chem. B* **2007**, *111*, 3325–3327.
29. Häkkinen, H.; Walter, M.; Grönbeck, H. Divide and Protect: Capping Gold Nanoclusters with Molecular Gold-Thiolate Rings. *J. Phys. Chem. B* **2006**, *110*, 9927–9931.
30. Grönbeck, H.; Walter, M.; Häkkinen, H. Theoretical Characterization of Cyclic Thiolated Gold Clusters. *J. Am. Chem. Soc.* **2006**, *128*, 10268–10275.
31. Jiang, D.-E.; Tiago, M. L.; Luo, W.; Dai, S. The "Staple" Motif: A Key to Stability of Thiolate-Protected Gold Nanoclusters. *J. Am. Chem. Soc.* **2008**, *130*, 2777–2779.
32. Mazzarello, R.; Cossaro, A.; Verdini, A.; Rousseau, R.; Casalis, L.; Danisman, M. F.; Floreano, L. S.; Morgante, A.; Scoles, G. Structure of a CH_3S Monolayer on Au(111) Solved by the Interplay between Molecular Dynamics Calculations and Diffraction Measurements. *Phys. Rev. Lett.* **2007**, *98*, 016102.
33. Wang, Y.; Hush, N. S.; Reimers, J. R. Formation of Gold-Methanethiyl Self-Assembled Monolayers. *J. Am. Chem. Soc.* **2007**, *129*, 14532–14533.
34. Grönbeck, H.; Curioni, A.; Andreoni, W. Thiols and Disulfides on the Au(111) Surface: The Headgroup−Gold Interaction. *J. Am. Chem. Soc.* **2000**, *122*, 3839–3842.
35. Andreoni, W.; Curioni, A.; Grönbeck, H. Density Functional Theory Approach to Thiols and Disulfides on Gold: Au(111) Surface and Clusters. *Int. J. Quantum Chem.* **2000**, *80*, 598–608.
36. Krüger, D.; Fuchs, H.; Rousseau, R.; Marx, D.; Parrinello, M. Interaction of Short-Chain Alkane Thiols and Thiolates with Small Gold Clusters: Adsorption Structures and Energetics. *J. Chem. Phys.* **2001**, *115*, 4776–4786.
37. Jadzinsky, P. D.; Calero, G.; Ackerson, C. J.; Bushnell, D. A.; Kornberg, R. D. Structure of a Thiol Monolayer-Protected Gold Nanoparticle at 1.1 Angstrom Resolution. *Science* **2007**, *318*, 430–433.
38. Whetten, R. L.; Price, R. C. Nano-Golden Order. *Science* **2007**, *318*, 407–408.
39. Cleveland, C. L.; Landman, U.; Schaaff, T. G.; Shafigullin, M. N.; Stephens, P. W.; Whetten, R. L. Structural Evolution of Smaller Gold Nanocrystals: The Truncated Decahedral Motif. *Phys. Rev. Lett.* **1997**, *79*, 1873–1876.
40. Knight, W. D.; Clemenger, K.; de Heer, W. A.; Saunders, W. A.; Chou, M. Y.; Cohen, M. L. Electronic Shell Structure and Abundances of Sodium Clusters. *Phys. Rev. Lett.* **1984**, *52*, 2141–2143.
41. de Heer, W. A.; Knight, W. D.; Chou, M. Y.; Cohen, M. L. In *Solid State Physics*; Ehrenreich, H., Seitz, F., Turnbull, D., Eds.; Academic Press: New York, 1987; Vol. 40, pp 94−180.
42. de Heer, W. A. The Physics of Simple Metal Clusters: Experimental Aspects and Simple Models. *Rev. Mod. Phys.* **1993**, *65*, 611–676.
43. de Heer, W. A. In *Metal Clusters at Surfaces*; Meiwes-Broer, K. H., Ed.; Springer: Berlin, 2000, pp 1−36.
44. Akola, J.; Walter, M.; Whetten, R. L.; Häkkinen, H.; Grönbeck, H. On the Structure of Thiolate-Protected Au_{25}. *J. Am. Chem. Soc.* **2008**, *130*, 3756–3757.
45. Heaven, M. W.; Dass, A.; White, P. S.; Holt, K. M.; Murray, R. W. Crystal Structure of the Gold Nanoparticle $[N(C_8H_{17})_4][Au_{25}(SCH_2CH_2Ph)_{18}]$. *J. Am. Chem. Soc.* **2008**, *130*, 3754–3755.
46. Zhu, M.; Aikens, C. M.; Hollander, F. J.; Schatz, G. C.; Jin, R. Correlating the Crystal Structure of A Thiol-Protected Au_{25} Cluster and Optical Properties. *J. Am. Chem. Soc.* **2008**, *130*, 5883–5885.
47. Tsunoyama, H.; Nickut, P.; Negishi, Y.; Al-Shamery, K.; Matsumoto, Y.; Tsukuda, T. Formation of Alkanethiolate-Protected Gold Clusters with Unprecedented Core Sizes in the Thiolation of Polymer-Stabilized Gold Clusters. *J. Phys. Chem. C* **2007**, *111*, 4153–4158.
48. Schaaff, T. G.; Shafigullin, M. N.; Khoury, J. T.; Vezmar, I.; Whetten, R. L.; Cullen, W. G.; First, P. N.; Gutiérrez-Wing, C.; Ascensio, J.; Jose-Yacamán, M. J. Isolation of Smaller Nanocrystal Au Molecules: Robust Quantum Effects in Optical Spectra. *J. Phys. Chem. B* **1997**, *101*, 7885–7891.
49. Garzón, I. L.; Reyes-Nava, J. A.; Rodríguez-Hernández, J. I.; Sigal, I.; Beltrán, M. R.; Michaelian, K. Chirality in Bare and Passivated Gold Nanoclusters. *Phys. Rev. B* **2002**, *66*, 073403.
50. Häkkinen, H.; Walter, M.; Gronbeck, H. Divide and Protect: Capping Gold Nanoclusters with Molecular Gold-Thiolate Rings. *J. Phys. Chem. B* **2006**, *110*, 9927–9931.
51. Häkkinen, H.; Barnett, R. N.; Landman, U. Electronic Structure of Passivated $Au_{38}(SCH_3)_{24}$ Nanocrystal. *Phys. Rev. Lett.* **1999**, *82*, 3264–3267.
52. Jiang, D. -E.; Tiago, M. L.; Luo, W.; Dai, S. The "Staple" Motif: A Key to Stability of Thiolate-Protected Gold Nanoclusters. *J. Am. Chem. Soc.* **2008**, *130*, 2777–2779.
53. Pei, Y.; Gao, Y.; Zeng, X. C. Structural Prediction of Thiolate-Protected Au_{38}: A Face-Fused Bi-icosahedral Au Core. *J. Am. Chem. Soc.* **2008**, *130*, 7830–7832.
54. Chaki, N. K.; Negishi, Y.; Tsunoyama, H.; Shichibu, Y.; Tsukuda, T. Ubiquitous 8 and 29 kDa Gold: Alkanethiolate Cluster Compounds: Mass-Spectrometric Determination of Molecular Formulas and Structural Implications. *J. Am. Chem. Soc.* DOI: 10.1021/ja8005379.
55. Mednikov, E.; Jewell, M. C.; Dahl, L. F. Nanosized $(\mu_{12}$-Pt)$Pd_{164-x}Pt_x(CO)_{72}(PPh_3)_{20}$ ($x \approx 7$) Containing Pt-Centered Four-Shell 165-Atom Pd−Pt Core with Unprecedented Intershell Bridging Carbonyl Ligands: Comparative Analysis of Icosahedral Shell-Growth Patterns with Geometrically Related $Pd_{145}(CO)_x(PEt_3)_{30}$ ($x \approx 60$) Containing Capped Three-Shell Pd_{145} Core. *J. Am. Chem. Soc.* **2007**, *129*, 11619–11630.
56. Johnson, C. L.; Snoeck, E.; Ezcurdia, M.; Rodrı´guez-González, B.; Pastoriza-Santos, I.; Liz-Marzán, L. M.; Hÿtch, M. Effects of Elastic Anisotropy on Strain Distributions in Decahedral Gold Nanoparticles. *Nat. Mater.* **2008**, *7*, 120–124.
57. Sánchez-Iglesias, A.; Pastoriza-Santos, I.; Pérez-Juste, J.; Rodrı´guez-González, B.; Garcı´a de Abajo, F. J.; Liz-Marzán, L. M. Synthesis and Optical Properties of Gold Nanodecahedra with Size Control. *Adv. Mater.* **2006**, *18*, 2529–2534.
58. Pastoriza-Santos, I.; Sanchez-Iglesias, A.; Garcia de Abajo, E. J.; Liz-Marzan, L. M. Environmental Optical Sensitivity of Gold Nanodecahedra. *Adv. Funct. Mater.* **2007**, *17*, 1443–1450.
59. Burke, K.; Perdew, J. P.; Wang, Y. In *Electronic Density Functional Theory: Recent Progress and New Directions*. Dobson, J. F., Vignale, G., Das, M. P., Eds; Plenum Publishing Corporation: New York, 1998.
60. Delley, B. An All-Electron Numerical Method for Solving the Local Density Functional for Polyatomic Molecules. *J. Chem. Phys.* **1990**, *92*, 508–517.
61. Delley, B. From Molecules to Solids with the $DMol^3$ Approach. *J. Chem. Phys.* **2000**, *113*, 7756–7764.